International Journal of Research Publication and Reviews

Journal homepage: www.ijrpr.com ISSN 2582-7421

Tuning the $Sr_5LaTi_3Nb_7O_{30}$-Based Oxide Thermoelectrics for Energy Harvesting

Adindu C. Iyasara [a], Victor D. Koreyo [b], Nobert O. Osonwa [c], Ben J. Robert [d], Chimezie V. Arinze[e]*

[a,b,c,c] Department of Ceramic and Glass Technology
[d] Department of Electrical and Electronics Engineering Technology
[e] Department of Mechanical Engineering Technology
AkanuIbiam Federal Polytechnic, Unwana, Nigeria

A B S T R A C T

A-site vacancy Sm-doped Sr5LaTi3Nb7O30 tetragonal tungsten bronze (TTB) ceramics codenamed SLTNvhave been investigated for their thermoelectric properties through vacancy doping using samarium (Sm) for energy harvesting. In this study, we report the synthesis and characterization of A-site deficient Sm-doped SLTNv ceramics with varying levels of Sm (x) compositions (x = 0.00, 0.05, 0.10, 0.1, 0.15, 0.20, 0.25, 0.30). The introduction of vacancies – strontium vacancy; oxygen vacancy (VSrand VO) in the lattice and the identified secondary phase mixture (SrTiO3 and Nb2O5) in the microstructure have been found to significantly alter electrical and thermal transport properties of the ceramics. The results show that thermoelectric figure of merit, ZT improved through careful control of the composition and microstructure. The enhanced thermoelectric performance is attributed to the increased electrical conductivity σ and reduced total thermal conductivity k, indicating that secondary phase mixture in the microstructure and the introduced vacancy defects in the lattice contributed in shortening the mean-free-path (MFP) of phonons, resulting in a reduced minimal k value of 1.6 W/m.K at 873 K and a maximum ZT of 0.21 at 973 K for x = 0.30 ceramic material.

Keywords: TTB ceramics, energy harvesting, vacancies, figure of merit, mean-free-path.

1. INTRODUCTION

Thermoelectric materials have the potential to convert waste heat into electrical energy, hence offering a promising solution for sustainable energy harvesting (Beil, 2008). Oxide ceramics such as perovskite, and TTB have emerged as a viable option for thermoelectric applications due to their high temperature stability, environmental friendliness and potential for improved performance through compositional tuning (Koumoto et al, 2013; Snyder et al, 2008).

The TTB structure is a complex framework lattice with a distorted, corner-sharing oxygen octahedra which forms three different tunnels or sites (Zhu et al, 2015; Fang et al, 2014; Smirnov & Saint-Grégoire, 2013). This structure has the capacity to accommodate large cations and possession of great flexibility for tuning the chemical composition. As a result of this structural arrangement, TTB shows excellent properties for diverse applications such as electro-optic, piezoelectric, pyroelectric, superconductivity and high permittivity (Zhu et al, 2015; Lin et al, 2014; Raju & Choudhary, 2003).

Thermoelectric properties of TTB oxides such as $Na_{18-x}W_{9+x}O_{47-\delta}$ and single crystal $Sr_xBa_{1-x}Nb_2O_{6-\delta}$ have been studied (Cerretti et al, 2017; Kieslich et al, 2016; Lee et al, 2012). With the results reported for these TTB compounds, it is obvious that TTB and other oxides with adaptive structures are potential candidates for thermoelectric applications (Kieslich, 2016).

In this study, Sr-site deficient Sm-doped $Sr_5LaTi_3Nb_7O_{30}$ TTB ceramics were explored for their thermoelectric properties with a view that vacancy doping using samarium (Sm) can significantly enhance their performance.

2. EXPERIMENTAL PROCEDURE

A-site deficient Sm-doped $Sr_{5-3x/2}Sm_xLaNb_7O_{30}$(x = 0.00, 0.05, 0.10, 0.15, 0.20, 0.25, 0.30) ceramics were synthesized using a solid state reaction method. The starting materials were $SrCO_3$ (Sigma-Aldrich, UK, 99.90 %), La_2O_3 (Sigma-Aldrich, UK, 99.99 % purity), TiO_2 (Sigma-Aldrich, UK, 99.90 %) and Nb_2O_5 (Stanford Mat. Corp. USA, 99.50 % purity). The stoichiometric properties of the powders were mixed and calcined in air at 1423 K for 6 h, followed by sintering in reducing atmosphere (H_2/N_2 gas) at 1673 K for 6 h.

The resulting ceramics were characterized for phase structure, microstructure and chemical composition using D2 Phaser Diffractometer (Bruker AXS GmbH, Germany), XL 30 S-FEG (Philips FEI) and energy dispersive X-ray Spectroscopy, EDX (INCA Energy EDS X-ray Microanalysis System, UK), respectively.

The thermoelectric (TE) properties were measured using a TE property measurement system. The electrical conductivity, $\boldsymbol{\sigma}$ and seebeck coefficient, S were measured simultaneously by employing Van Der Pauw 4-point probe method using SBA-458 Nemesis instrument (NETZSCH-GeratabauambH Germany). The thermal conductivity, k was measured using a thermal properties analyzer, AnterFlashline TM 3000, Pittsburgh, PA 15235, USA. With the combined values of the $\boldsymbol{\sigma}$, S and k, the dimensionless thermoelectric figure of merit, ZT was calculated.

3. RESULTS AND DISCUSSION

3.1 Phase Assemblage and Microstructure

The results of x-ray diffraction studies (Fig. 1) confirmed all prepared $Sr_{5-3x/2}Sm_xLaNb_7O_{30}$ (x = 0.00, 0.05, 0.10, 0.15, 0.20, 0.25, 0.30) ceramics are indexed with the $Sr_5LaTi_3Nb_7O_{30}$ TTB structure for the major peaks. Secondary phases with ideal $SrTiO_3$ perovskite and Nb_2O_5 were detected. The presence of these secondary phases is attributed to structural instability induced by oxygen deficiency, V_o (Deng et al, 2017).

All prepared ceramic samples showed similar microstructure with a bimodal grain size distribution as shown in Fig. 2. The small grains indicated the presence of second phase dispersed within the large grains and at grain boundaries. This therefore is a conformation of secondary phases as identified in the XRD result. The grain size of the large grains ranges from ~ 4 to 5 µm while the secondary phases are typically 1 – 2 µm in size.

Combined SEM/EDX studies performed on the ceramics confirmed the composition of the large grains to be TTB phase while the smaller grains of similar contrast are $SrTiO_3$ with the smallest bright grains being Nb_2O_5 (Fig.3).

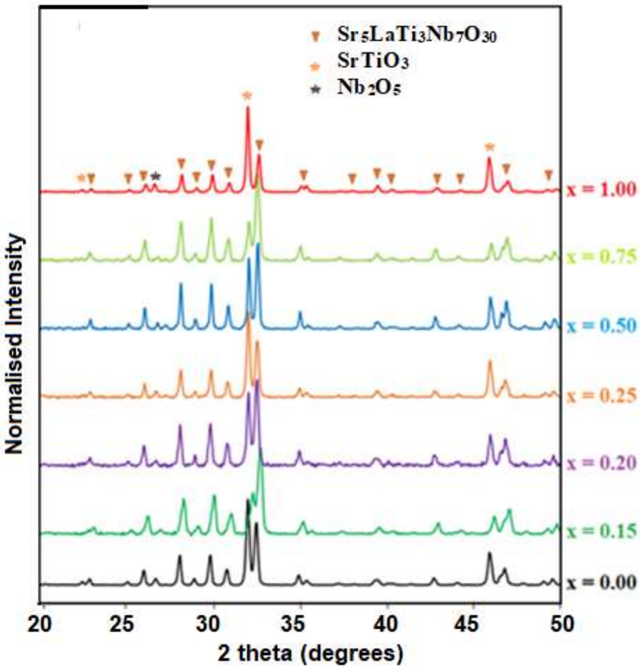

Fig. 1. Room temperature XRD patterns of SLTNv ceramics sintered in 5% H_2/N_2 gas at 1673 K for 6 h

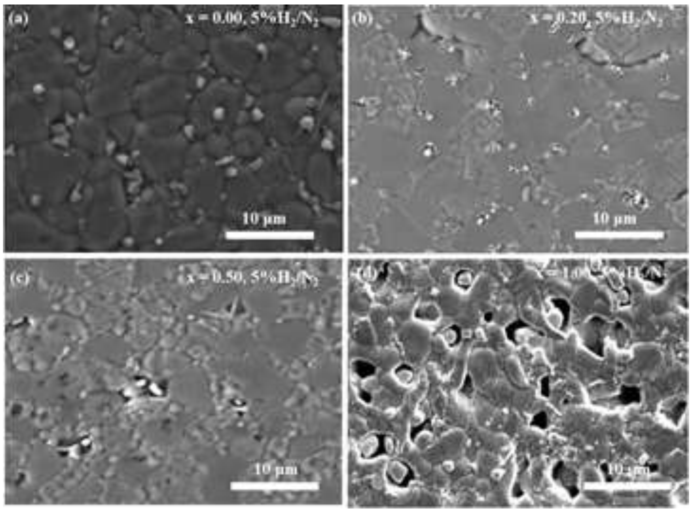

Fig. 2.SEM micrographs of SLTNv ceramicssintered in 5% H_2N_2gas at 1673 K for 6 h

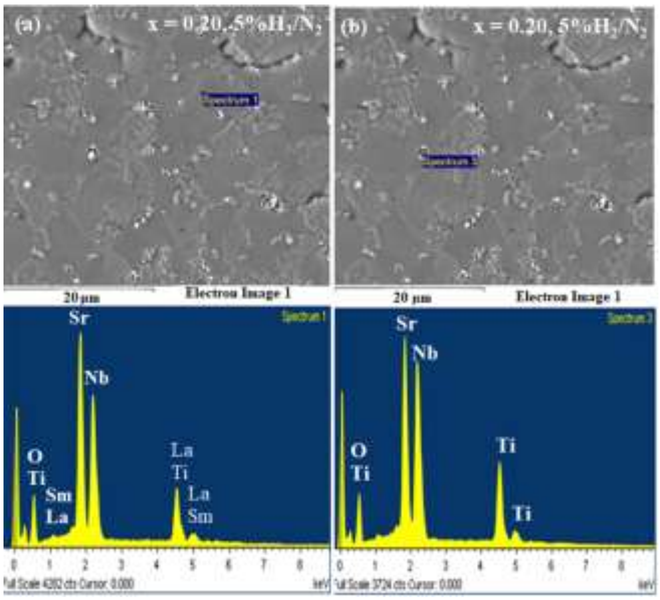

Fig. 3. EDX trace of SLTNvceramics sintered 6 hours in 5% H2/N2 at 1673 K from a (a) large grain, TTB phase (spectrum 1) (b) small grain or secondary phase (spectrum 3).

3.2 Electrical Transport Properties

Fig.4 shows the temperature dependence of the electrical conductivity, σ of the SLTNv ceramics sintered 5% H_2N_2 gas at 1673 K for 6 h. The σ behavior is divided into two parts: part I and part II for discussion purposes.

The electrical conductivity of part I (x = 0.00, 0.15, 0.20) is higher than part II (x = 0.05, 0.10, 0.25, 0.30). The σ of part I ceramic samples exhibited a peak behavior in the low temperature range (573 – 773 K), showing a semiconductor-like behaviour, and transits to metallic behaviour at the maximum temperature, 973 K (Wang et al, 2011; Muta, Kurosaki, & Yamanaka, 2015).In contrast, all ceramic samples in part II showed a progressive increase between 573 K and 873 K and decreased at 973 K. The highest σ (~ 292 S/cm) was recorded for x = 0.20 ceramic at 673 K.

The absolute Seebeck coefficient, $|S|$ of SLTNv ceramics as a function of temperature is shown in Fig. 5. The S of all ceramics are negative, indicating that electrons are the dominant carriers. It also increased linearly with increasing temperature, and this is attributed to an increase in the internal entropy (Cerretti et al, 2017). The highest S recorded for SLTNv ceramics is 164 µV/K (for x = 0.30) at 973 K.

The thermoelectric power factors (PF) of SLTNv ceramics is shown in Fig.6. The highest PF is expected to occur in x = 0.20 ceramics with the highest σ (~ 292 S/cm). In contrast, x = 0.00 ceramics (undoped sample) showed the highest PF value, 417 $\mu W/K^2$ at 973 K. It, therefore, shows that Sm doping does improve the PF of SLTNv compositions. It is argued that the improved PF is as a result of the presence of the secondary phases particularly the $SrTiO_3$ phase in the microstructure. This assertion is supported by the work of Lu et al (2015) on La-doped $Sr_3Ti_2O_7$Ruddlesden-Pepper (RP) ceramics. They showed that compositions with $SrTiO_3$ secondary phases resulted in high PF.

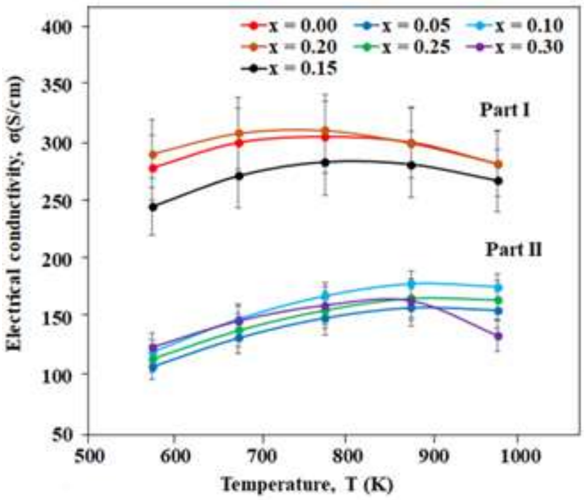

Fig.4. Temperature dependence of electrical conductivity for SLTNv ceramics sintered in 5% H_2/N_2 at 1673 K for 6 h

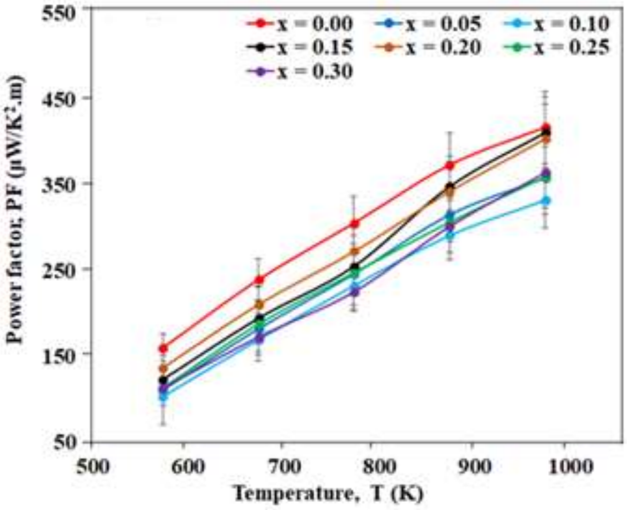

Fig.6. Temperature dependence of Power factor for SLTNv ceramics sintered in 5% H_2/N_2 at 1673 K for 6 h

3.3 Thermal Transport Properties

The total thermal conductivity, k of SLTNv ceramics is shown in Fig.7. k of all samples vary irregularly with Sm concentration especially at low temperatures. This anomaly could be due to the influence of numerous factors such as defect scattering, bond angles of the Ti-O and Nb-O octahedral; and changes in phase assemblage as a function of composition. At low temperatures, majority of of the thermally excited phases possess small momentum, and this is known as Normal process (N-process) (Spiteri, 20150). As a result, momentum is conserved, thus no effect on net energy, momentum contribution, scattering in heat transport and mean free path for k. hence, increase in k with temperature.

All ceramics exhibited low k values (1.62 – 3.85 W/m.K) in the whole measured temperature range. This observation suggests that the presence of secondary phases ($SrTiO_3$ and Nb_2O_5) in the microstructure and the vacancy defects (V_{Sr} and V_O) act as scattering centres, shorten the MFP of phonons and restrict their propagation, resulting in a decrease in k. x = 0.30 ceramics showed the lowest k (~ 1.6 W/m.K) at 873 K.

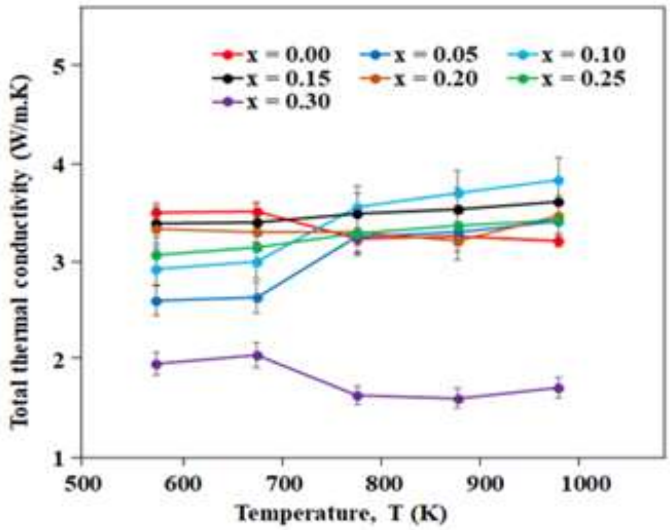

Fig.7. Temperature dependence of total thermal conductivity for SLTNv

ceramics sintered in 5% H_2/N_2 at 1673 K 6 h.

3.4 Thermoelectric Figure-of-Merit

The overall thermoelectric performance or efficiency of A-site vacancy Sm-doped $Sr_5LaTi_3Nb_7O_{30}$ ceramics investigated was measured using the thermoelectric figure of merit, ZT. The ZT as a function of temperature is shown in Fig.8.

The ZT values of all the ceramics increased with temperature in the measured temperature range. The highest ZT, 0.21 was observed in $Sr_{4.55}LaSm_{0.30}Ti_3Nb_7O_{30}(x = 0.30)$ceramics at 973 K. Equally the $x = 0.30$ ceramics recorded the smallest total thermal conductivity (k) value of 1.6 W/m.K at 873 K. Therefore, the secondary phase inclusions ($SrTiO_3$ and Nb_2O_5) observed in the microstructure and the created vacancy defects (V_{Sr} and V_O) in the lattice would have contributed to the enhancement of phonon scattering. The overall impact therefore, is the decrease in k which results in increase in ZT.

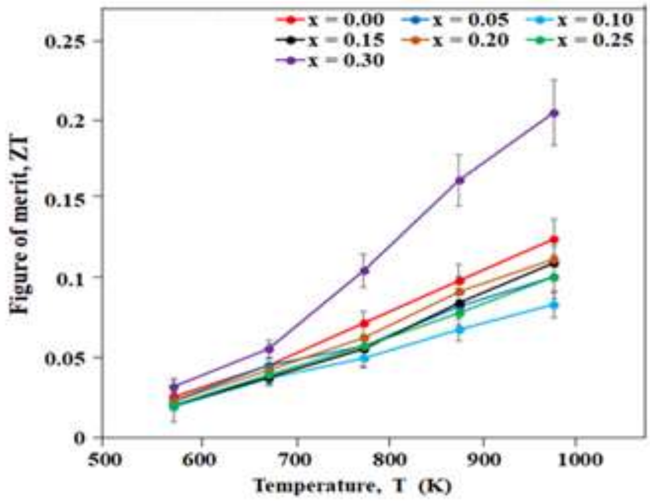

Fig. 8. Temperature dependence of thermoelectric figure of merit for SLTNv

Ceramics sintered in 5% H_2/N_2 at 1673 K. 6 h.

4. CONCLUSION

*$Sr_{5-3x/2}Sm_xLaNb_7O_{30}$ (x = 0.00, 0.05, 0.10, 0.15, 0.20, 0.25, 0.30)*TTB ceramics were prepared via a conventional solid state route, followed by sintering in a 5%H_2/95%N_2 atmosphere at 1673 K for 6 h. Their thermoelectric properties were assessed at 573 K < T<973 K in the same atmosphere. The study demonstrates that tuning the thermoelectric properties via vacancy doping using a samarium (Sm) rare earth element is a promising approach for developing high performance thermoelectric materials for energy harvesting.

The enhanced ZT is attributed to the created A-site and oxygen vacancies in the lattice and the consequent secondary phase mixture in the microstructure. These therefore result in the increase and decrease observed in the electrical conductivity and thermal conductivity, respectively of the ceramics. As a result, a highest ZT value of 0.21 and lowest k value of 1.6 W/m.K were achieved in $Sr_{4.55}LaSm_{0.30}Ti_3Nb_7O_{30}(x = 0.30)$ceramics at 973 K and 873 K, respectively.

A further systematic research is recommended to optimize the composition and microstructure of these ceramic materials and to explore their potential applications in sustainable energy harvesting.

Acknowledgements

The authors also acknowledge the characterisation carried out at the Functional Materials and Devices Laboratory and the Sorby Centre, Department of Materials Science and Engineering, The University of Sheffield, UK.

References

Bao Li Deng, Xiao Li Zhu, Xiao Qiang Liu, & Xiang Ming Chen, (2017). Effects of oxygen-deficiency on crystal structure, dielectric and ferroelectric properties in Sr_5 $SmTi_{3+2x}Nb_{7-2x}O_{30-x}$ with tungsten bronze structure, *RSC Adv.*, 7 (44), 27370–27376.

Cerretti, G ; Schrade, M; Song, X; Balke, B ; Lu, H; Weidner, T; Lieberwirth, I; Panthöfer, M; Norby, T & Tremel, W, (2017). Thermal stability and enhanced thermoelectric properties of the tetragonal tungsten bronzes $Nb_{8-x}W_{9+x}O_{47}$ (0 < x < 5). *J. Mater. Chem. A*, 5 (20), 9768–9774.

David Spiteri, (2015). Understanding phonon scattering and predicting thermal conductivity from molecular dynamics simulation. PhD Thesis, University of Bristol.

Gregor Kieslich, Giacomo Cerretti, Igor Veremchuk, Raphaël P. Hermann, Martin Panthöfer, Juri Grin, and Wolfgang Tremel, (2016). A chemists view: Metal oxides with adaptive structures for thermoelectric applications. *Phys. Status Solidi Appl. Mater. Sci.*, 213 (3), 808–823.

Hiroaki Muta, Ken Kurosaki, & Shinsuke Yamanaka, (2005). Thermoelectric properties of reduced and La-doped single-crystalline $SrTiO_3$. *J. Alloys Compd.*, 392 (1–2), 306–309.

Hong Chao Wang, Chun Lei Wang, Wen Bin Su, Jian Liu, Yi Sun, Hua Peng, & Liang Mo Mei, (2011). Doping effect of La and Dy on the thermoelectric properties of $SrTiO_3$,. *J. Am. Ceram. Soc.*, 94 (3), 838–842.

Jason H. Chan, Jonathan A. Bock, Hanzheng Guo, Susan Trolier-McKinstry, & Clive A. Randall, (2017). Filled oxygen-deficient strontium barium niobates. *J. Am. Ceram. Soc.*, 100 (2) 774–782.

Kun Lin, Yangchun Rong, Hui Wu, Qingzhen Huang, Li You, Yang Ren, Longlong Fan, Jun Chen, & Xianran Xing, (2014). Ordered Structure and Thermal Expansion in Tungsten Bronze Pb_2 $K_{0.5}Li_{0.5}Nb_5O_{15}$. *Inorg. Chem.*, 53, (17), 9174–9180.

Raju, M.R.R & Choudhary, R.N.P, (2003). Diffuse phase transition in $Sr_5RTi_3Nb_7O_{30}$ (R=La, Nd and Sm)," *J. Phys. Chem. Solids*, 64 (5), 847–853.

Smirnov, M & Saint-Grégoire, P, (2013). An innovative approach to structural instabilities in tetragonal tungsten bronze crystals through the concept of rigid unit modes. *Condens. Matter*, 1–22.

Soonil Lee, Jonathan A. Bock, Susan Trolier-McKinstry, & Clive A. Randall, (2012). Ferroelectric-thermoelectricity and Mott transition of ferroelectric oxides with high electronic conductivity. *Journal of the European Ceramic Society*, 32 (16), 3971–3988.

Yu Jiao Fang, Gao Shang Gong, Zerihun Gebru, & Song Liu Yuan, (2014). Effects of A1 site occupation on dielectric and ferroelectric properties of $Sr_4CaRTi_3Nb_7O_{30}$ (R = Ce, Eu) tungsten bronze ceramics. *Chinese Phys. B*, 23(12).

Zhilun Lu, Derek C. Sinclair, Ian M. Reaney, & X. Tan, (2016). The Influence of La Doping and Heterogeneity on the Thermoelectric Properties of $Sr_3Ti_2O_7$ Ceramics. *J. Am. Ceram. Soc.*, 99 (2) , 515–522.

Zhu, X; Fu, M; Stennett,M.C; Vilarinho, P. M ; Levin, I; Randall, C.A; Gardner,J; F. D.

Morrison, F.D & Reaney, I.M, (2015). A Crystal-chemical framework for relaxor versus normal ferroelectric behavior in tetragonal tungsten bronzes," *Chem. Mater.*, 27(9), 3250–3261.